Numerical evaluation of an external environment effectiveness to the surface plasmon mode in Au slot waveguide for design the sensor simulation

Pattrapong Racknoi*

Department of Physics, Faculty of Arts and Science, Kasetsart University, Kampangsean Campus, Nakornpatom, 73140 Thailand

***Corresponding Author:** faasptr@ku.ac.th
https://doi.org/10.55674/jmsae.v11i3.249088

Received: 22 July 2022 | **Revised:** 28 August 2022 | **Accepted:** 20 January 2023 | **Available online:** 1 May 2023

Abstract

The effective permittivity of gold thin films with an external thin dielectric layer on the top and core of the slot waveguide was evaluated as an effective compound semi-metal layer of the surface plasmonic polariton slot waveguide that will vary due to some environmental factors. By uses simple parallel and series permittivity of compound material, this value need for the computation of the effective propagating vector β_{sp}. This takes for a sensor model designing which the external environment effectiveness was changed by the surface plasmonic mode in its slot waveguide. So the resonance length and grating period are evaluated for the sensor model in the first. Further, the propagation of the SPP surface wave mode along the interface between the compound cladding and Si dielectric waveguide is computed, while the effective refractive index of the compound cladding of the slot waveguide is increased from 1 − 1.50. The computation results showed that the TM_0 mode power transfer and propagation length seem to vary with this effective refractive index of the compound cladding on the surface plasmonic polariton waveguide. The 140 nm gap width and 3.70 μm long waveguide is also simulated by the finite different time domain method in the optiwave program, where the TM_0 mode transition output is corrected, while the refractive index of the environment layer is changed. The results of the simulation showed good agreement with the computation in that the TM_0 mode depends on the external refractive of index and input wavelength. This result shows that loss peak ships vary with the external refractive index thin film layer and input wavelength. Thus, they seem to be useful for sensor applications such as the solution concentration analytic.

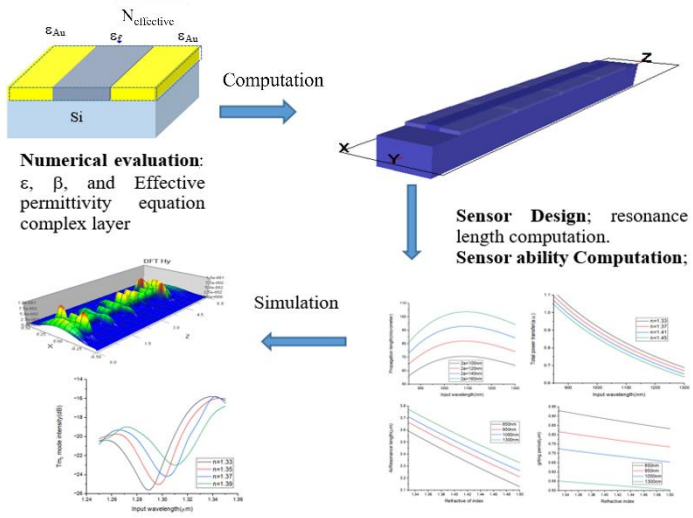

Keywords: Array waveguide grating; Nanograting; Plasmonic sensor; Polariton

Introduction

The resonance wave at the interface between the thin metal film and dielectric is called the Surface Plasmon Polariton (SPP), which the transverse magnetic (TM) mode is oscillating at the metal-dielectric interface even though the input transverse electric (TE) mode can't pass through this waveguide. For many years, SPP waveguides have been reported in many branches of research such as optics and photonics, [1 − 4] optoelectronics, [5 − 7] nanosensor, [8 − 12] communications [13 − 16], metamaterials

[9], and nanotechnology [14, 16]. Many prototypes of SPP devices and waveguides have been researched over the years. The slot waveguide has been a popular model used in SPP waveguide research. The waveguide was previously designed as a metal-dielectric metal SPP slot waveguide, called an MDM slot waveguide. Globally, this waveguide

has been applied in sensor and device research [1 − 16]. Many researchers have tried to prove that the inner effect of SPP single slot waveguide shows the possibility of using nano sensors and nano devices [1 − 2, 16 − 18], but this research trends to prove that the external effective permittivity may be included with metal thin films as single compound thin slot of waveguide that may be changed by the external environments such as chemical absorption or thermal inducing. So the compound effective permittivity of Au thin film and dielectric core layer is computed in simple local parallel and perpendicular polarization equation that the model of single slot sensor is designed as resonance length. And the model consists of 2 and 4 arrays of single slot lines along the waveguide that has a small space gap between each slot is also proved by grating period computation. The SPP TM_0 power transfer mode is evaluated which assumes that thin metal and external environment gaps are compounded together which has an only effective permittivity of only a thin layer slot that is placed on the Si substrate. The computation result shows that the SPP mode seems to vary with the external permittivity of the environment gap. The simulation model is designed from computation value and the simulation with changing gap refractive index is simulated that TM_0 mode output is corrected for graph plotting between TM_0 mode intensity and the external refractive index gap, which is changed from 1 − 1.50 (this value corresponds to some solution as seem to be real environment) The input wavelength is also changed from 850 – 1,500 nm in the simulation (this wavelength is active IR SPP wavelength of gold) , and the result of the situation shows good agreement within the computation. This shows the ability for sensor applications though there are some loss peaks which ship by the changing of the refractive index of external thin layer adding. In addition, many slot waveguides seem to be more sensitive than a single slot. This may be helpful to the SPP sensor model design before simulation and fabrication.

The electric field along the metal dielectric metal (MDM) slot waveguide, as in Fig. 1(a), is an equation of time and z component;

$$E_z(t) = E_z(x)e^{j\omega t - j\beta z} \quad (1)$$

where t is a time, ω is the resonance angular frequency, β is a propagation vector and the electric field in function of x in z component $E_Z(x)$ can be expressed in the condition:

$$E_z(x) = \begin{cases} E_0 sinh(\gamma x + \varphi), & |x| \le a \\ E_0 sinh(\gamma a + \varphi)e^{-\alpha_c(x-a)}, & x \ge a \\ -E_0 sinh(\gamma a - \varphi)e^{\alpha_s(x+a)}, & x \le -a \end{cases} \quad (2)$$

E_0 is an dielectric amplitude, a is the dielectric gap width, γ is the propagation vector in x component of dielectric core, α_s and α_c are the propagation vector in x component of two Au claddings, which $\gamma a + \varphi = atanh\left(-\frac{p_c\alpha_c}{\gamma}\right)$ and $\gamma a - \varphi = atanh\left(-\frac{p_s\alpha_s}{\gamma}\right) - jm\pi$, $p_s = \frac{\varepsilon_f}{\varepsilon_s}$, $p_c = \frac{\varepsilon_f}{\varepsilon_c}$ and εf is an dielectric permittivity, ε_c and ε_s are the two cladding permittivity, and

$$\gamma = \sqrt{\beta^2 - k_0^2\varepsilon_f}, \alpha_c = \sqrt{\beta^2 - k_0^2\varepsilon_c}, \ \alpha_s = \sqrt{\beta^2 - k_0^2\varepsilon_s} \quad (3)$$

k_0 is a propagating vector of electromagnetic wave in free space in z direction

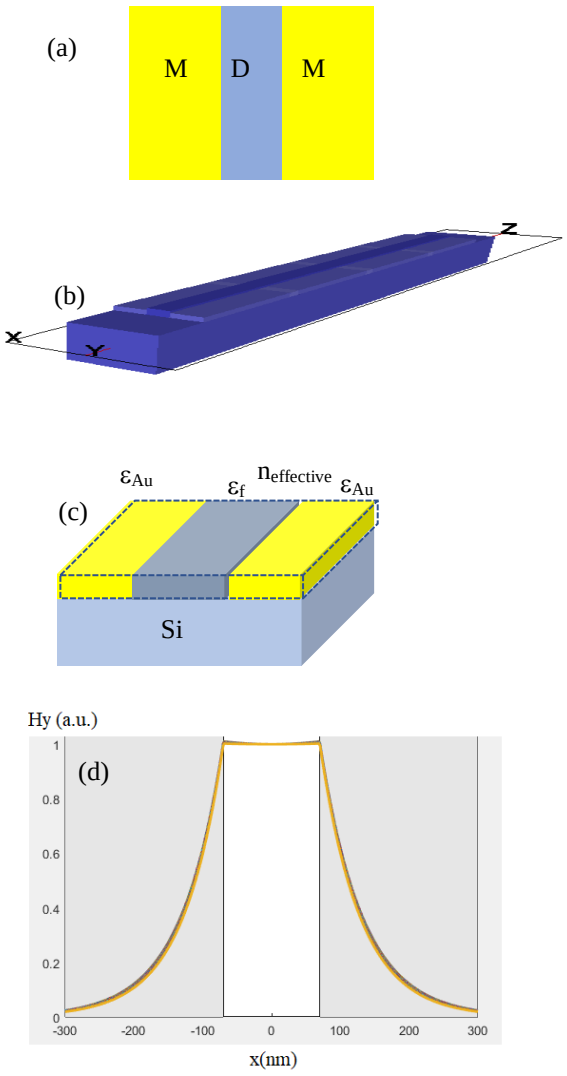

Fig. 1 shows the model of the waveguide and certain properties in the model including (a) MDM waveguide, (b) model of SPP slots line waveguide, (c) effective value of the

permittivity for the cladding of the waveguide and (d) H_y TM_0 mode.

The electric field of this waveguide is in the form of eq. (4);

$$E_x = -\frac{j\beta}{-\gamma^2}\partial_x E_z \quad (4)$$

while the magnetic field of TM_0 mode in the slot waveguide is eq. (5);

$$H_y = \frac{1}{\eta_{TM}}E_x, \eta_{TM} = \frac{\beta}{\omega\varepsilon_0\varepsilon_f} \quad (5)$$

while TM_0 mode in y direction wave shows as in eq. (6);

$$H_y(x)\begin{cases} H_0 cosh(\gamma x + \varphi), & |x| \le a \\ H_0 cosh(\gamma a + \varphi)e^{-\alpha_c(x-a)}, & x \ge a \\ -H_0 cosh(\gamma a - \varphi)e^{\alpha_s(x+a)}, & x \le -a \end{cases} \quad (6)$$

TM_0 mode cut off depends on the width of the gap slot as a function of eq. (7);

$$\gamma = -\frac{\gamma^2 + p_c\alpha_c p_s\alpha_s}{p_c\alpha_c + p_s\alpha_s} tanh(2\gamma a) \quad (7)$$

ε_f=1 if it is the free space gap and $\varepsilon_s = \varepsilon_c = \varepsilon_{Au}$ (permittivity of gold) in this MDM waveguide. All these equations were evaluated by the MATLAB program, which has many useful support functions to evaluate certain values such as β, γ, power transfer in the waveguide, cut-off gap width and propagation length.

Materials and Methods

The Lorenz-Drude dispersion materials equation is computed for the permittivity of the metal surface that can be expressed in the form of eq. (8);

$$\varepsilon_r(\omega) = \varepsilon_{r,\infty} + \sum_{m=0}^{M}\frac{G_m\Omega_m^2}{\omega_m^2 - \omega^2 + j\omega\Gamma_m} \quad (8)$$

where $\varepsilon_{r,\infty}$ is the relative permittivity in the infinity frequency, Ω_m is the plasma frequency, ω_m is the resonant frequency, and Γ_m is the damping factor or collision frequency. In this study, the ε_m in the β equation is computed from the approximation value of this equation that has a table of all six orders of Au in the optiwave manual. This value is also used for evaluating the effective refractive index of MDM cladding for the slots waveguide as a compound cladding in Fig. 1(c). The refractive index of core dielectric is about 1.33 − 1.50 for some dielectrics such as solution, silicone, and thermal polymer [19] which is changed by the environment in this study. The β value is evaluated for TM_0 power mode transfer, and propagation length is verified for sensitivity to the effective refractive index changing of compound cladding. The oscillation length ($L_z = \frac{\pi}{2\beta}$) and grating period length (L_g) of the sensor ($\beta_{sau}(L_g - L_{sp}) + \beta_{sp}L_{sp} = (2m+1)\pi$ are computed for the sensor designing that use in the simulation model. While β_{sau} is propagating vector in gold slot length, L_g is the grating length and L_{sp} is the space length and β_{sp} is the propagating vector in space. The β_{sau} is also evaluated in from Au/Au solution permittivity which step of concentration change is 0.01 %. If L_{sp} = 0.10 μm and m = 0, so grating length is

$$L_g = \frac{\pi - \beta_{sp}L_{sp}}{\beta_{sau}} - 0.1 \quad (9)$$

In the simulation model within finite difference time domain method algorithm, this value is embedded in optiwave software; we must take all terms in the table in the optiwave manual as a parameter of the object properties of gold in the SPP waveguide. The gap refractive index of the model in Fig. 1(b) is usually constant, but it may be changed by external effects in some cases such as chemical reactions, polymer heating in the gap, and chemical absorption, which could be useful for some environment sensor applications.

Results and Discussions

Microstructure characterization

The results of the computation in MATLAB show a good gap width that is used for the sensor model from about 50− 150 nm for 1,100 − 1,500 nm input wavelength. The TM_0 mode is not cut off in this range, as in Fig. 2, A graph of an effective refractive index increased rapidly at near the narrow gap in all of the wavelength inputs as in Fig. 2(a). Since the effective refractive of index trends to maximum when the gap width is close to zero, non-slope of graph lines at more than 200 nm gap width, so the good selection in gap width of design sensor model should be 50 – 100 nm. This gap width varies less than the cut-off TM_0

mode gap width, even though its refractive index is changed from 1 − 1.50 (with 0.01 in each step) as in the computation of the TM_0 mode cutoff in Fig. 2(b).

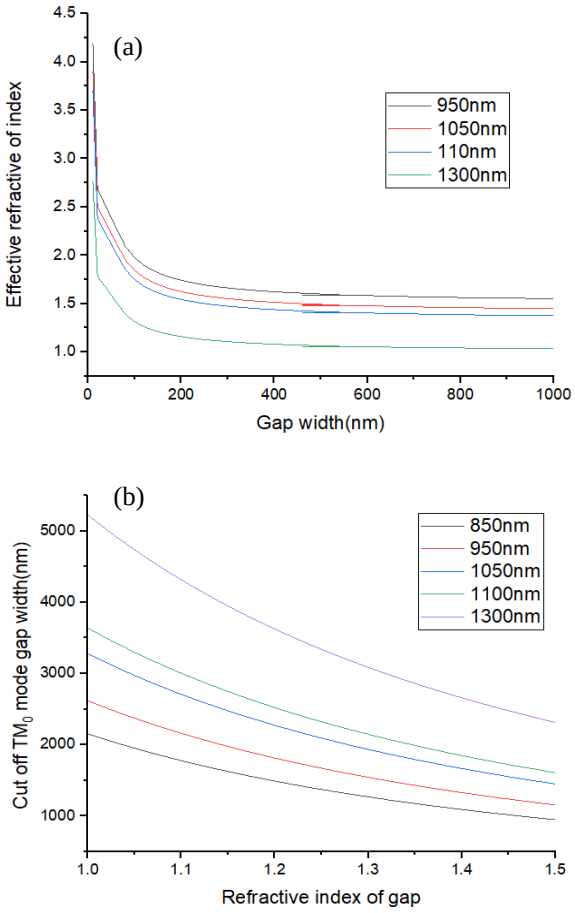

Fig. 2 the computation result of, (a) the relation between the effective refractive index of waveguide depends on gap dielectric (10 nm in each step), the gap width near zero to 200 nm is the best, and (b) the relation between the cutoff TM_0 gap width and core refractive index (0.01 in each step) at IR wavelengths from 850 nm to 1,300 nm.

This shows that the relation between the cutoff TM_0 gap width and the core refractive index of some IR wavelengths is linear. It is also shown that TM_0 mode cutoff vary to input wavelength. Also, in the relation between the propagation length of surface plasmonic mode and input wavelength at some core refractive index shows a curve that it depends on the gap refractive index and gap width as in Fig. 3. This shows that the propagation length computation of the SPP mode in the waveguide longer than 3.75 μm of the design sensor length by more than ten times, which is long enough to cover a range that is changed by the refractive index of the gap from 1.33 − 1.50, even though the input wavelength is changed from 850 − 1,500 nm and gap width from 100 − 160 nm, as in Fig. 3a to Fig. 3d. The result of the computation in Fig. 4 shows very clearly that the propagation length of the SPP mode varies increasingly with gap width as in Fig. 4(a) and depends on input wavelength covering all 850 nm – 1,500 nm as in Fig 4(b). For the narrow gap width of about 100 − 200 nm with a 1.33 gap refractive index, the propagation length is a nearly smooth curve, as in Fig. 4(a). This gives a situation gap width for the sensor model in the simulation. The good computation result shown in Fig. 4(b) reveals that the propagation length decreases linearly according to the gap refractive of index at some near IR input wavelength, the best slope in the graph is 1,300 nm input wavelength. The propagation length of the SPP mode decreases with gap refractive index covering all 1 − 1.50. This decreasing is not the problem for the designing model, since the important property is power transfer and situation sensor length. The power transfer of the SPP mode is also dependent on the input wavelength at some gap refractive index, as shown in Fig. 5; the rapid decrease of power transfer varies with input wavelength for all gap widths of 100 nm, 140 nm and 160 nm in Fig. 5(a) − 5(c) that has best power transfers in narrowest gap width, but not much difference between in each gap refractive index. Thus, the two-gap refractive index of the SPP waveguide is fixed at 1 and 1.33, while the gap width and input wavelength are varied. The results show more significance for sensitivity to input wavelength, as in Fig 6(a) and 6(b). The best computation for power transfer in Fig. 6(a) shows that it depends on the change of gap refractivity from about 1 to be 1.33 in the gap. This results reveal that there is more difference in total power transfer for each value of the gap width in the waveguide and shows the significance about 0.0009 Arb.unit/nm and 0.0008 Arb.unit/nm that depends on the gap refractive index. This show good sensitivity to the input wavelength, and gap refractive of index changing. This shows good significance in the sensor model. So the resonance length L_z of only the Au single slot sensor waveguide is computed for sensor designing and the result is shown in Fig. 7(a). And the single slot waveguide with 50%:50% per volume of thin Au layer and dielectric thin layer on the top that the result shows as in Fig. 7(b). This show the best importance for the simulation, that the result of 4 times of resonance length L_z computation is about 3.10 – 4.00 μm. Then the resonance length of the 4 slots was determined for both only Au and Au : dielectric (Au : D) type, the result shows that its length near about 3.50 μm to 4.20 μm as in Fig. 8 both all of only AU thin film only

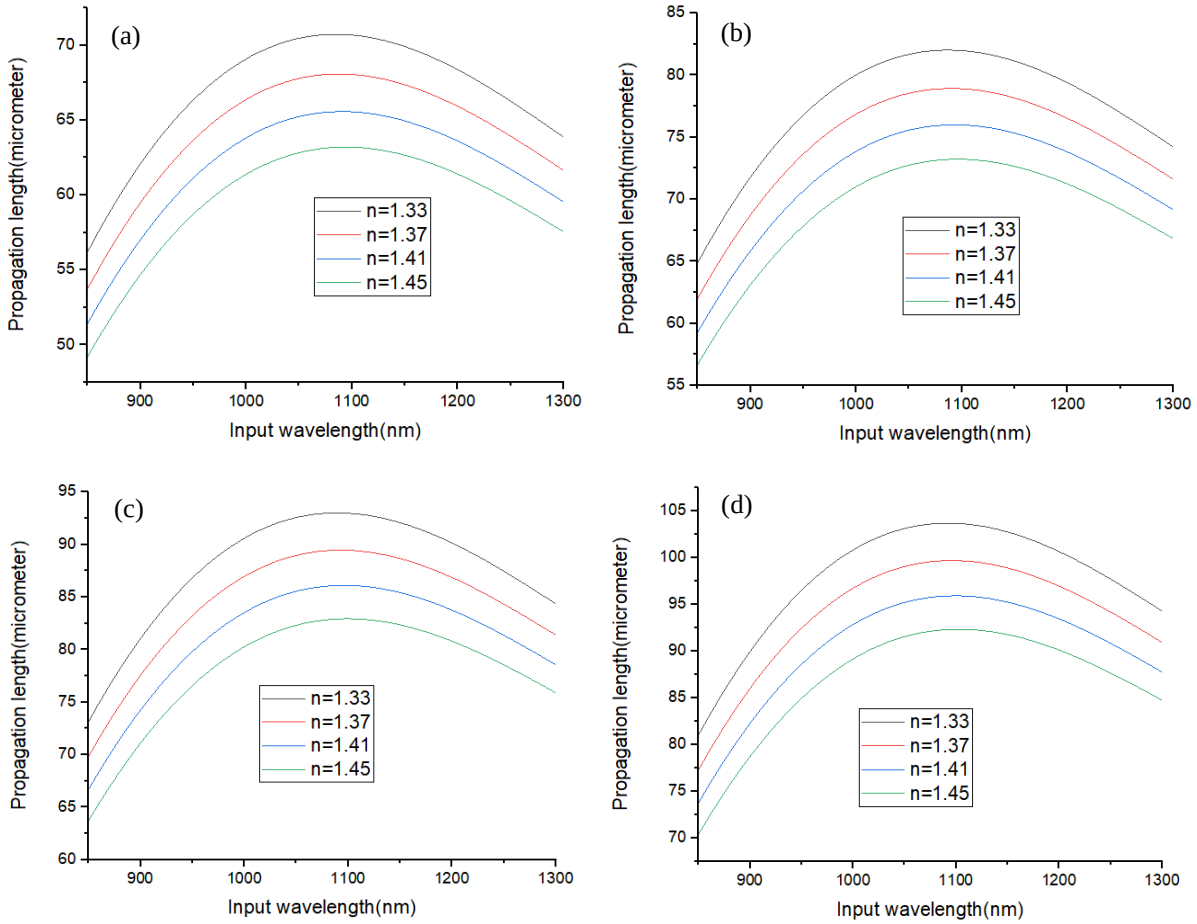

Fig. 3 The computation results of the relation between propagation lengths of plasmonic and wavelengths (10 nm in each step) at some core refractive of index for a gap width is (a) 100 nm, (b) 120 nm, (c) 140 nm, and (d) 160 nm.

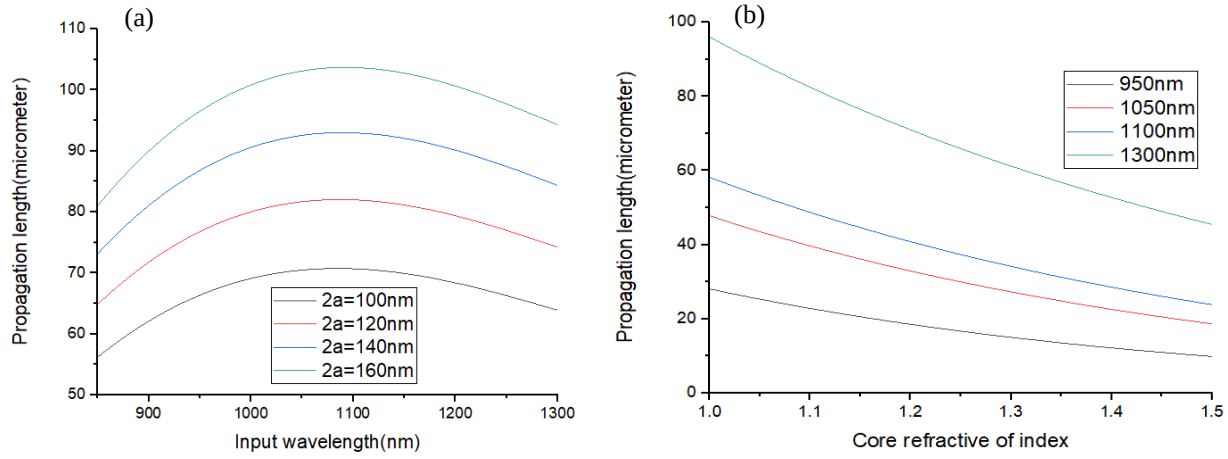

Fig. 4 The computation results of (a) the relation between propagation lengths of plasmonic and wavelengths (10 nm in each step) at 1.33 core refractive of index for a gap width are 2a = 100, 2a = 120, 2a = 140, and 2a = 160 nm and (b) the relation between propagation lengths of plasmonic and core refractive of index (0.01 in each step) at some wavelength for a 140 nm gap length.

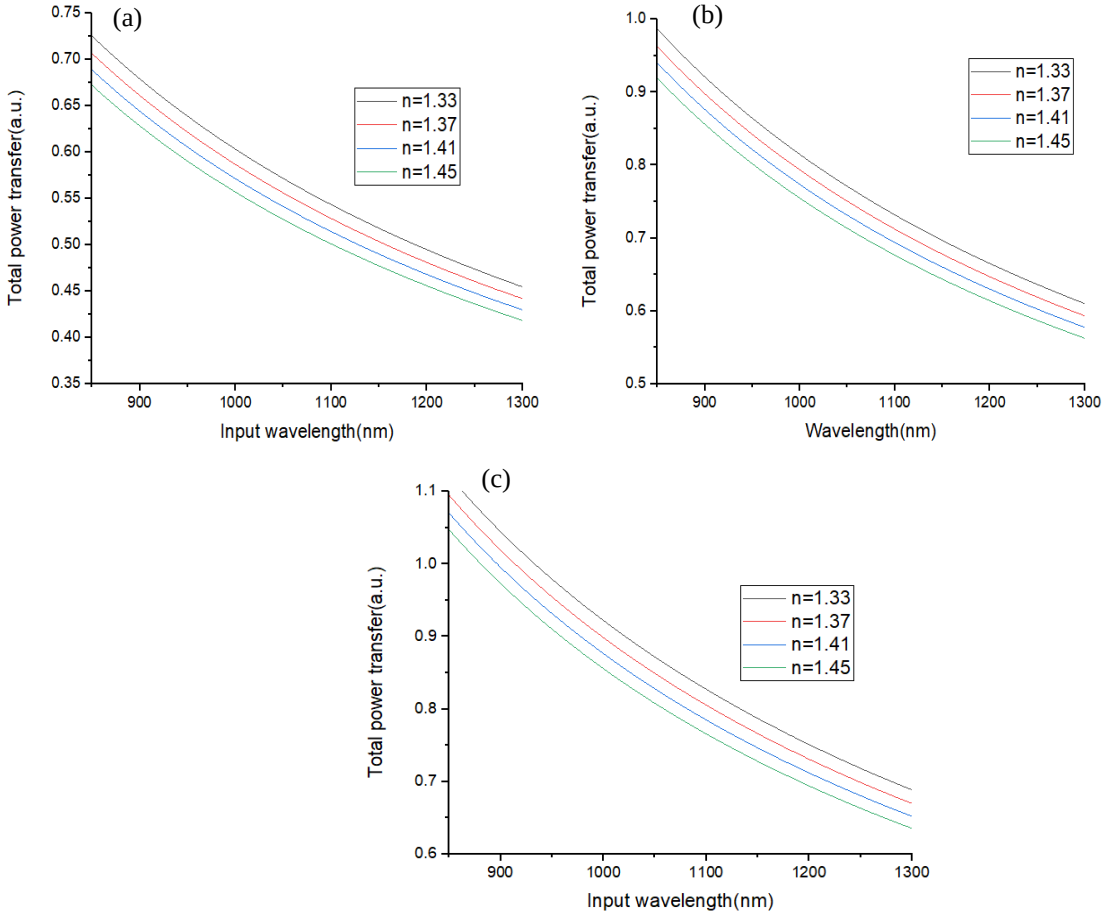

Fig. 5 The computation results of the relation between power transfer in gap and wavelength (10 nm in each step) at some core refractive of indexes with gap widths of (a) 100 nm, (b) 140 nm, and (c)160 nm.

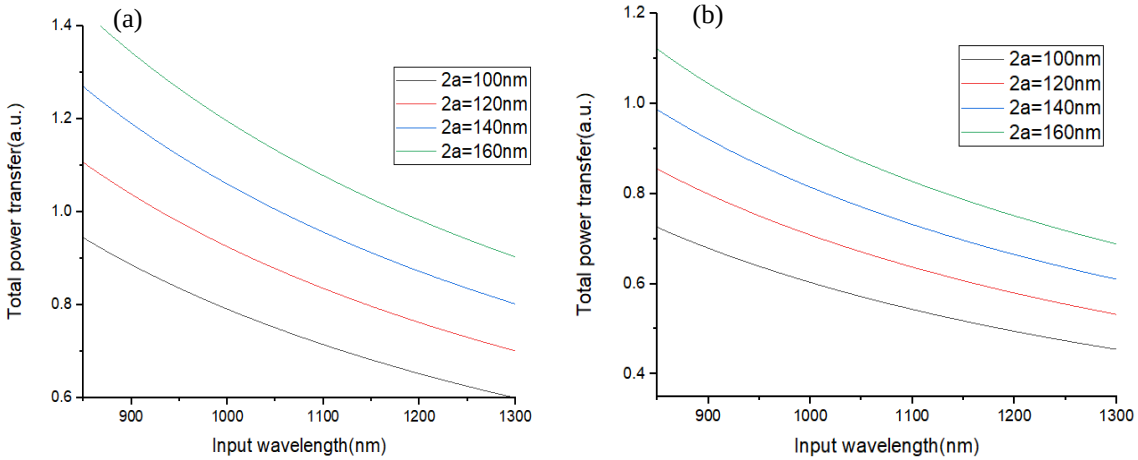

Fig. 6 The computation results of the relation between power transfer and wavelength (10 nm in each step) with gap widths of 2a = 100 nm, 2a = 120 nm, 2a = 140 nm and 2a = 160 nm at core refractive indexes of (a) 1 and (b) 1.33.

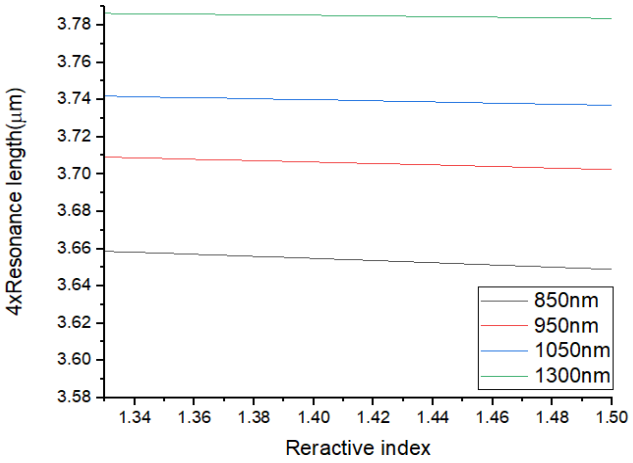

a) form only thin Au

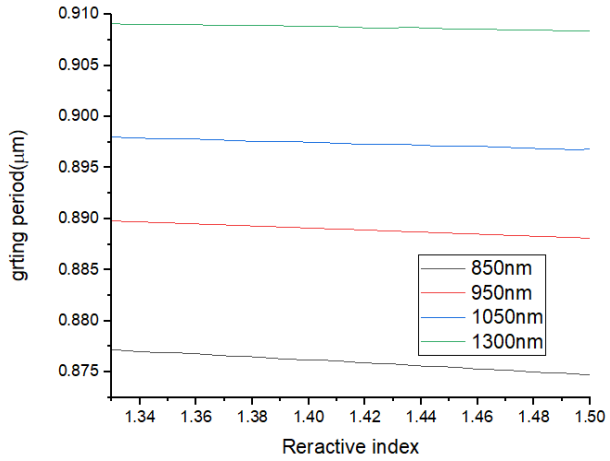

(b) form thin 50 : 50 of Au : D

Fig. 7 The result of sensor length design which was computed in each input wavelength and refractive index (0.01 in each step) (a) from resonance length equation of single Au slot and (b) from grating period length equation of four slots (about ¼ of sensor length).

(Fig.8(a)) and 50%:50% of Au with dielectric on the top (Fig. 8(b)). And the grating period L_g of 4 Au only slots like grating manner sensor waveguide is evaluated that the result show as in Fig. 9(a), and in Fig 9b was the result of Au thin film with dielectric layer on the top that the 4 times of L_g was nearly to 3.50 – 4.00 μm. So the 3.75 μm model length is selected in the simulation model which is best easily designed. In addition, the active sensor length was designed, Fig 7 − 9 show that a 140 nm gap width with 3.50 − 4 μm long can be a model of the sensor in which the refractive index is changed by an environment.

These shows agree well together in both the l_z and L_g equation. Thus, the 3.75 μm is about 4 times of mean of L_g and L_z computation value that is good for the simulation model. This design was proved by the simulation result, this show the possibility of sensor applications for the model, as in Fig. 10(a). This picture shows the TM_0 mode which oscillates along a slot waveguide, this mode is the near field intensity of surface wave at the output of the waveguide which is directly read on screen. The SPP TM_0 of the single slot model in Fig. 10(a) is corrected while the gap refractive index of the slot is about 1.33 − 1.48 with 0.01 in each step that the four input wavelength was simulated, as in Fig. 10(b). Their result shows that there is a difference in the sensitive region of gap refractive index, but not enough benefit for sensor application.

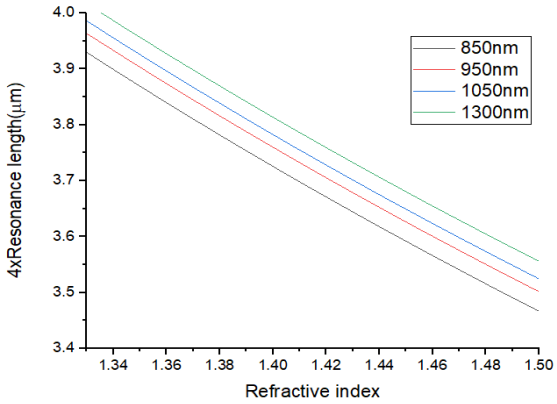

(a) form only thin Au

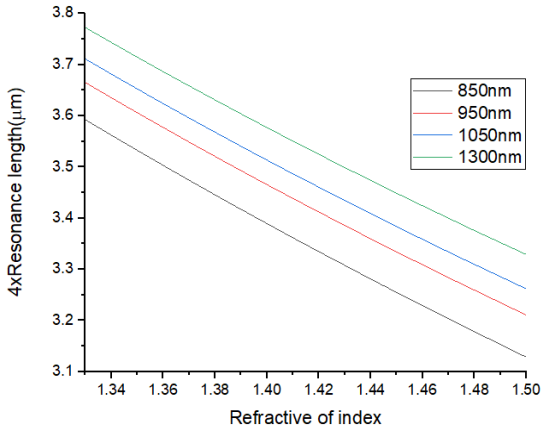

(b) form thin 50 : 50 of Au : Dielectric

Fig. 8 The computation results of resonance length of 4 slot line, that has verity core refractive index (0.01 in each step) at some wavelengths which 4 times of resonance length computed of slot waveguide, (a) with only Au thin film and (b) with thin Au and dielectric on the top.

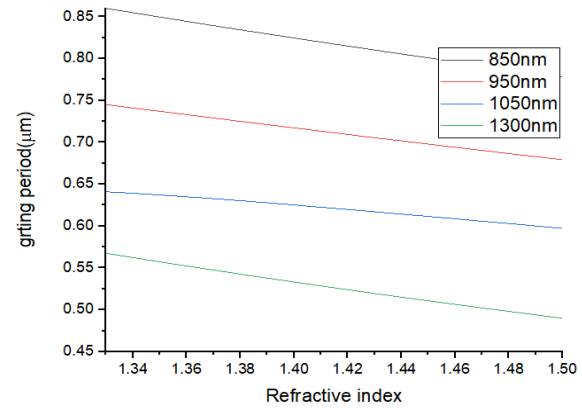

(a) form only thin Au

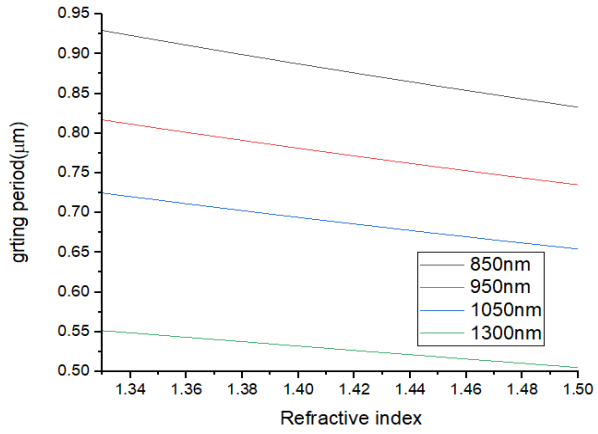

(b) form thin 50 : 50 of Au:Dielectric

Fig. 9 The grating period of the computation results of 4 slots, that that has verity core refractive of index (0.01 in each step) at some wavelengths which was computed one period, (a) form only Au thin slot and (b) form thin Au with dielectric on the top.

For a single slot, it has less sensitivity than in the simulation of the two and four slots, as in Fig. 11, which shows slope and loss peaks that seem to have an effective refractive index of gap dielectric layer changing. This shows that more slots seem to enable more slope and deep loss peaks. Furthermore, the slope and peak seem to depend on input wavelength, as in Fig. 11(a) and 11(b), so the shipping of loss peak is very good in Fig. 11(b) at 1,300 nm input wavelength. It has more shipping of gap refractive index than in Fig. 11(a), and it seems that the loss peak of the 4 is deeper than in the 2 slots and the single slot. This shows that TM_0 mode intensity is effected by the gap refractive index. The dielectric liquid solution layer was added for improving the environmental sensitivity of the sensor as in simulation results shown in Fig 12(a) reveal that some thin layers form as a thin environmental layer, which shows that the ship of loss peak depends on the external environment refractive of index and input wavelength. This shows that there are many loss peaks along with the 850 − 1,450 nm input wavelength, which seems to show more sensitivity of TM_0 mode in SPP with the environment layer on the gold thin films. Furthermore, Fig. 12(b) shows that the SPP environment sensors model may be beneficial as it has a ship of loss peak vary to some refractive index of thin-film layer in some short-range input wavelengths. This was improved by the result of the simulation with lower step input wavelengths. The loss of peak shipping depends on the external environment and the effectiveness permittivity of layers**.**This seems beneficial for sensor applications. So this sensor model also shows good sensitivity to environmental changing by an external factor such as temperature or other chemical refractive index.

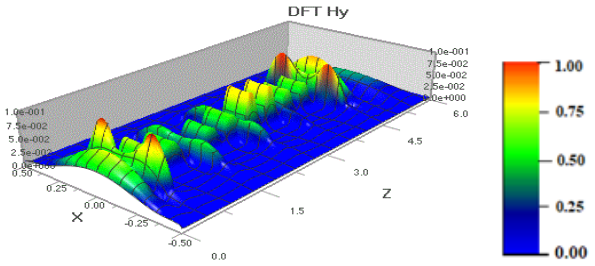

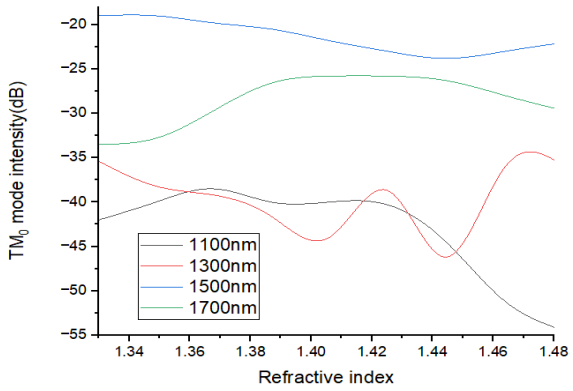

Fig. 10 The results of the simulation, (a) TM mode along the waveguide gap is simulated that shows SPP mode oscillations along the waveguide and (b) The simulation results show the graph of TM_0 mode H_y field intensity (dB), and refractive index (0.01in each step) of the gap at some wavelength inputs from 1.10 − 1.70 μm of the single slot with only thin Au films.

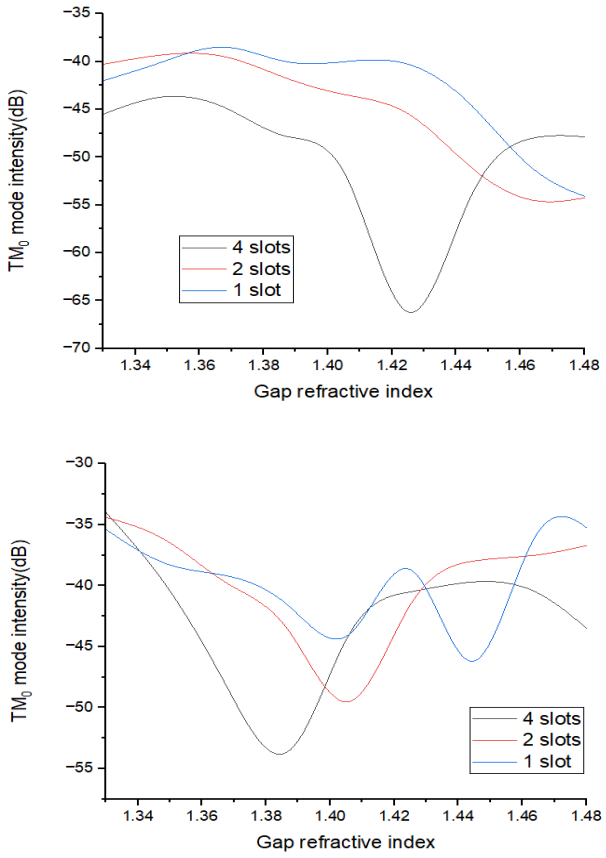

Fig. 11 The simulation results for the graph of TM_0 mode H_y field intensity (dB), and refractive of index (0.01 in each step) of the gap at some wavelength inputs (a) 1.10 μm and (b) 1.30 μm.

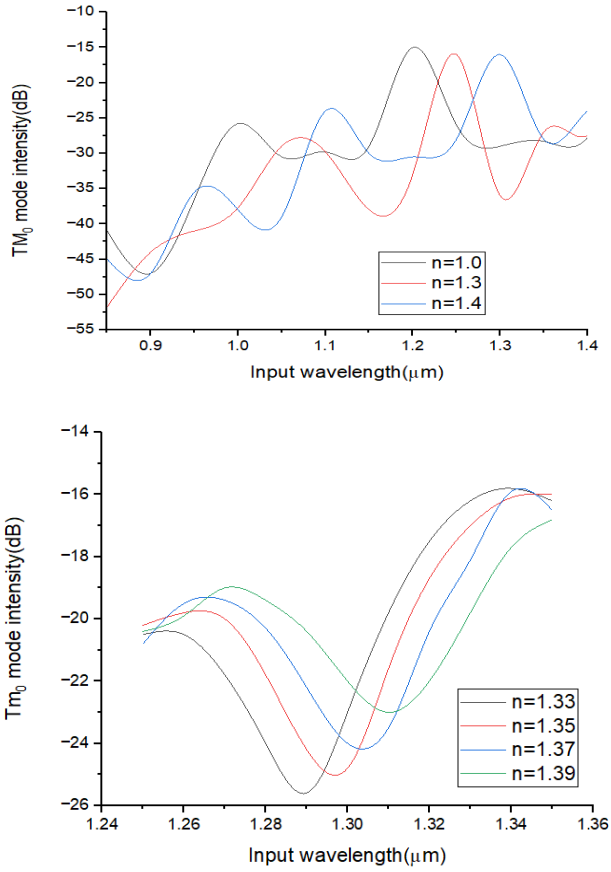

Fig. 12 Relation between the intensity of TM_0 (dB) and input wavelength (10 nm in each step) at some external refractive index layers, (a) long range input wavelength and (b) short range input wavelength, on some external refractive of index layers.

Conclusion

The computation result of some values of the MDM SPP slot waveguide sensor such as effective refractive index, mode cutoff, sensor length, propagation length, and SPP power transfer seem to offer a suitable sensor model that is approved for sensor applications with 3.75μm and 140 nm gap width of the simulation model. This model has some effect on the gap refractive of the index (from 1 − 1.50) by the external environment at low IR input (from 850 – 1,500 nm). This sensitivity seems to agree well with the computation and simulation. It may be a sensor model with an effect on the change of external environment layer on the waveguide such as a temperature sensor or chemical absorption sensor. This must be a further study that will use a new bester metal thin film and new good sensitive gap material.

Acknowledgement

The authors would like to thank the staff at Kasetsart University for supporting the use of its laboratory facilities.

References

[1] N.T. Huong, N.V. Chinh, C.M. Hoang, Wedge Surface Plasmon Polariton Waveguides Based on Wet-Bulk Micromachining, Photonics. 6(1) (2019) 21.

[2] P. N. Melentiev, A. Kalmykov, A. Kuzin, D. Negrov, V. Klimov, V. I. Balykin, Open-Type SPP Waveguide with Ultrahigh Bandwidth up to 3.5 THz, Photonics. 6 (2019) 1425.

[3] S. Kumari, S. Gupta, Performance Estimation of Hybrid Plasmonic Waveguide in Presence of Stress. Plasmonics. 16(2021) 359.

[4] A. M. Shrivastav, U. Cvelbar, I. Abdulhalim, A comprehensive review on plasmonic-based biosensors used in viral diagnostics, Communications Biology) 4(70) (2021) 1.

[5] A. Andryieuski, A.V. Zenin, R. Malureanu, S. V.Volkov, I. S. Bozhevolnyi, V.A. Lavrinenko, Direct Characterization of Plasmonic Slot Waveguides and Nano couplers, Nano Letters. 14 (2014) 3925.

[6] J.R .Salgueiro, Y.S. Kivshar, Nonlinear couplers with tapered plasmonic waveguides. Optics Express. 20 (2012) 9403.

[7] Y. Fu, X. Hu, C. Lu, S. Yue, H. Yang, G. Qihuang, All Optical Logic Gates Based on Nanoscale Plasmonic Slot Waveguides, Nano Letters. 12 (2012) 5784.

[8] V.A. Zenin, V.S. V., Z. Han, S. L .Bozhevolnyi, E. Devaux, T.W. Ebbesen, Directional coupling in channel plasmon polariton waveguides, Optics Express. 20 (2012) 6124.

[9] C., S. Li, H. Sun, Metamaterials Application in Sensing, Sensors. 12(2012) 2742.

[10] Y. Chen, H. Ming, Review of Surface Plasmon Resonance and Localized Surface Plasmon Resonance Sensor, Photonic Sensors. 2 (2012) 37.

[11] T. Wang, C. Tu, F. Liu, H. Chen, Surface Plasmon Resonance Waveguide Biosensor by Bipolarization Wavelength Interrogation, IEEE Photonics Technology Letters. 16 (2004) 1715.

[12] G. D. Osowiecki, E. B., A. Naqavi, H. P. Herzig, Vertically Coupled Plasmonic Slot Waveguide Cavity for Localized Bio-sensing applications, Optics Express. 22 (2014) 20871.

[13] Z. Han, A. Y. Elezzabi, V. Van, Wideband Y-splitter and aperture-assisted coupler based on sub-diffraction confined plasmonic slot waveguides, Applied Physics Letters. 96 (2010) 131106-1.

[14] C. Delacour, S. Blaize, P. Grosse, J. M. Fedeli, A. l. Bruyant, R. Salas-Montiel, G. Lerondel, A. Chelnokov, Efficient Directional Coupling between Silicon and Copper Plasmonic Nano slot Waveguides: toward Metal-Oxide-Silicon Nanophotonics, Nano Letters. 10(2000) 2922.

[15] Z. Zhu, C. E. Garcia-Ortiz, Z. Han, I. P. Radko, S. I Bozhevolnyi, Compact and Broadband Directional Coupling and Demultiplexing in Dielectric-loaded Surface Plasmon Polariton Waveguides Based on the Multimode Interference Effect, Applied Physics Letters. 103 (2013) 061108-1.

[16] C. Du, Y. Chiou, Vertical Directional Couplers with Ultra-Short Coupling Length Based on Hybrid Plasmonic Waveguides, Journal of Lightwave Technology. 32 (2014) 2065.